Structural Durability & Health Monitoring

Tech Science Press

https://doi.org/10.32604/sdhm.2026.083328

ARTICLE

Bond Behavior of NPR Bar/Steel Strands with Ultra-High-Performance Concrete

Qinfeng Pan[1], Wei Zhang[1], Hao Chen[1], Lin Pang[2], Xiang Liu[1,*] and Chun Chieh Yip[3]

[1]School of Civil Engineering, Fujian University of Technology, Fuzhou, China
[2]China Railway Eryuan Engineering Group Co., Ltd., Chengdu, China
[3]Department of Civil Engineering, Universiti Tunku Abdul Rahman, Bandar Sungai Long, Cheras, Kajang, Selangor, Malaysia

*Corresponding Author: Xiang Liu. Email: liuxiang@fjut.edu.cn

Received: 01 April 2026; Accepted: 06 May 2026; Published: 30 June 2026

ABSTRACT: Ultra-high-performance concrete (UHPC) exhibits high strength, toughness, and durability, making it an excellent candidate for integration with novel high-ductility, high-strength negative Poisson's ratio (NPR) steel bars. This combination shows promising applications in the fields of bridges and buildings. This study investigates the bonding performance of various types of NPR bars (smooth NPR bars, spiral rib NPR bars, and NPR steel strands) with UHPC as the concrete matrix. It examines the effects of bond length, bar diameter, and NPR bar type on bonding performance, comparing these results with those of normal concrete (NC). A predictive model for the bonding performance of NPR bars with UHPC was developed. Results show that in the UHPC matrix, all types of NPR bars primarily exhibit pullout failure, with bond strength exceeding that of the NC matrix group by 47.07%. The use of NPR bars improves ductility, with all groups demonstrating better ultimate slip compared to traditional steel bars. An increase in bond length reduces the ultimate strength of all NPR bar types while simultaneously increasing ultimate slip. Similarly, a larger bar diameter decreases the ultimate strength of NPR steel strands by 32.32% and increases slip. During this process, the expansion effect of the strand wires complicates the loading conditions during pullout. Among the three NPR bar types, spiral rib NPR bars exhibit the highest ultimate strength but relatively low slip. In contrast, smooth NPR bars and NPR steel strands have lower ultimate strength but allow for greater slip. The parameter, empirical, and composite models developed in this study demonstrate strong predictive accuracy, with most models achieving an R^2 value above 0.7. These models reliably estimate the ultimate strength and slip of NPR bars in UHPC. These findings provide a solid theoretical foundation and practical guidance for the application of NPR bars in UHPC.

KEYWORDS: NPR reinforcement; UHPC; bond behavior; failure mode; bond-slip constitutive model

1 Introduction

The tensile yielding of steel reinforcement during service presents a significant concern in reinforced concrete structures, as it involves early-stage necking that can lead to premature structural failure and associated safety risks. To address this issue, numerous researchers have adopted various types of novel reinforcing bars, including CFRP bars [1], GFRP bars [2] and epoxy-coated reinforcement bars [3], and advanced high-strength steel bars [4]. Among these, He et al. [5] developed a type of steel reinforcement exhibiting a negative Poisson's ratio effect, termed Negative Poisson's Ratio (NPR) reinforcement. NPR reinforcement outperforms conventional steel bars in ductility, corrosion resistance, and resistance to magnetization, with an elongation after fracture exceeding 30% [6,7]. According to the material tests in this study, the elongation of smooth NPR bars can even surpass 50%. Moreover, NPR bars exhibit negligible

necking upon fracture, whereas hot-rolled steel bars undergo pronounced necking. This exceptional uniform elongation is primarily attributed to the synergistic effects of mechanical twinning (TWIP effect) [8–10] and transformation-induced plasticity (TRIP effect) from retained austenite [11,12], which impart a high and sustained strain-hardening capacity to the material.

Extensive research has been conducted to facilitate the application of NPR reinforcement across various fields. Fundamental investigations have further elucidated its microstructural mechanisms and exceptional plasticity [8,11,12]. Concurrently, significant attention has been directed toward the interfacial bond behavior of NPR reinforcement. For instance, investigations have covered its bonding properties in normal and marine concrete environments [6,13,14], as well as the influence of bar surface geometry [15]. Additionally, recent studies have systematically explored its bonding mechanisms and constitutive models when embedded in UHPC matrices [7,16,17]. At the macroscopic structural level, a variety of applications have been explored, ranging from component-level dynamic and static performance [17–19] to specific geotechnical engineering solutions [5]. In terms of flexural behavior, Zheng et al. [20] employed NPR bars as both longitudinal and stirrup reinforcement in concrete beams, achieving increases of 2.4% and 21.8% in cracking load and peak load, respectively, along with a 1.7-fold enhancement in energy ductility coefficient. With respect to high-performance matrices, Gu et al. [18] reported that NPR reinforcement enhanced the flexural strength of UHPC beams by 47.8%–55.2% and improved deformability by up to 1.8 times. Zhang et al. [21] further elucidated the underlying mechanism, demonstrating that NPR reinforcement transformed the failure mode from brittle "over-reinforced shear compression" to ductile "flexural-shear compression." Regarding seismic performance and energy dissipation, Long et al. [19] confirmed that NPR-UHPC beams achieved drift ratios exceeding 8% under cyclic loading, indicating outstanding energy dissipation capacity. In the field of geotechnical anchorage, He et al. [5] showed that quasi-NPR steel bolts outperformed conventional bolts by factors of 3.5 and 3.68 in shear deformation capacity and energy absorption, respectively, underscoring their substantial engineering potential.

Recent findings on the bond behavior between NPR reinforcement and concrete are summarized in Table 1. Shao et al. [6] observed that although the initial bond strength of NPR bars in marine concrete is approximately 25% lower than that of HRB400 bars, increasing the concrete strength grade from C30 to C50 can enhance bond strength by up to 40%. Zhou et al. [14] further investigated the effect of corrosion level, revealing that bond strength initially increases and then decreases with corrosion severity, peaking at a corrosion rate of approximately 1.8%. In terms of geometric characteristics and detailing, Xiong et al. [15] demonstrated that increasing the number of helical grooves on NPR bars from three to six significantly improves bond performance, whereas longer anchorage lengths lead to a reduction in average bond strength. Meanwhile, Li et al. [13] reported the positive effect of stirrup ratio on ultimate pullout load and identified 41 times the bar diameter as the critical anchorage length. With respect to dynamic response and fatigue behavior, Lu et al. [22] showed through cyclic loading tests that NPR reinforcement exhibits superior energy dissipation capacity and enhanced fatigue resistance compared to conventional HRB635 and HRB400 bars.

Table 1: NPR pulls out experimental research data.

Specimen	Concrete Type	f_{cu} (MPa)	Vf (%)	Reinforcing Bar Diameter (mm)	Anchorage Length (mm)	NPR Type	Bond Stress (MPa)	Bond Slip (mm)	Failure Mode	Source
NPR 2.5% 3d	UHPC	153.2	2.5	16	48	T4	55.12	1.53	P	Lu et al. [17]
NPR 2% 3d	UHPC	139.6	2	16	48	T4	46.29	1.29	P	
NPR 1% 3d	UHPC	128.5	1	16	48	T4	43.08	0.61	SP	
NPR 0–3d	UHPC	86.2	0	16	48	T4	31.34	0.38	S	
NPR 2.5% 4d	UHPC	153.2	2.5	16	64	T4	47.16	1.99	P	
NPR 2.5% 5d	UHPC	153.2	2.5	16	80	T4	40	1.64	P	
NPR 2.5% 6d	UHPC	153.2	2.5	16	96	T4	37.1	1.42	P	
NPR 2.5% 3d	UHPC	153.2	2.5	16	48	T4	47.43	0.85	P	
NPR 2.5% 3d	UHPC	153.2	2.5	16	48	T4	50.51	0.96	P	
NPR 2.5% 3d	UHPC	153.2	2.5	16	48	T4	51.46	1.06	P	
NPRA 2.5% 3d	UHPC	153.2	2.5	16	48	T4	50.76	0.88	P	
NPRB 2.5% 3d	UHPC	153.2	2.5	16	48	T4	55.11	2.51	P	
A	UHPC	133.97	2.2	16	16	T4	52.59	0.5	P	Lu et al. [22]
RR	UHPC	133.97	2.2	16	32	T4	50.56	0.62	P	
B	UHPC	133.97	2.2	16	48	T4	49.42	0.8	P	
C	UHPC	133.97	2.2	16	64	T4	44.62	1.16	P	
D	UHPC	133.97	2.2	16	80	T4	43.1	1.51	P	
2	UHPC	133.97	2.2	16	96	T4	37.18	1.77	P	
E	UHPC	133.97	2.2	16	48	T4	45.03	0.61	P	
F	UHPC	133.97	2.2	16	48	T4	51.74	0.95	P	
G	UHPC	133.97	2.2	16	48	T4	53.99	1.11	P	
H	UHPC	113.34	0	16	48	T4	40.78	0.23	SP	
I	UHPC	121	0.5	16	48	T4	41.6	0.58	SP	
J	UHPC	125.4	1.2	16	48	T4	45.68	0.7	SP	
K	UHPC	133.97	2.2	16	48	T4	35.01	0.42	S	
L	UHPC	133.97	2.2	16	48	T4	43.1	0.7	SP	
M	UHPC	133.97	2.2	16	48	T4	45.06	1.52	P	
N	UHPC	133.97	2.2	16	48	T4	54.25	0.44	P	
O	UHPC	133.97	2.2	12.6	37.8	T4	41.33	2.76	P	
P	UHPC	133.97	2.2	12	36	T4	50.06	2.11	P	
Q	UHPC	133.97	2.2	12	36	T4	55.42	1.45	P	
N08/5 d/30	NC	34.2	0	8	40	T2	8.95	4.84	P	Shao et al. [6]
N18/5 d/30	NC	34.2	0	18	90	T2	13.29	3.56	S	
N18/7 d/30	NC	34.2	0	18	126	T2	10.59	2.96	S	
N08/5 d/40	NC	49.2	0	8	40	T2	8.81	3.04	P	
N18-5 d-40	NC	49.2	0	18	90	T2	14.30	3.50	S	
N18/7 d/40	NC	49.2	0	18	126	T2	12.34	3.22	S	
N08/5 d/50	NC	63.4	0	8	40	T2	27.86	5.10	P	
N18/5 d/50	NC	63.4	0	18	90	T2	17.43	3.07	S	
N18/7 d/50	NC	63.4	0	18	126	T2	16.12	2.97	S	
C3-17-5d	NC	43.3	0	17	85	T2	12.6	1.83	P	Xiong et al. [15]
C6-17-5d	NC	43.3	0	17	85	T2	14.63	2.21	S	
N-5d-0%	NC	36.7	0	18	90	T2	9.59	2.24	S	Zhou et al. [14]
N-7d-0%	NC	36.7	0	18	126	T2	8.41	2.3	S	

Note: T2 represents spiral-ribbed NPR reinforcement; T4 represents ribbed NPR reinforcement.

Ultra-High-Performance Concrete (UHPC) is a cementitious material recognized for its outstanding mechanical properties, achieved through optimized mixture proportions and the incorporation of

high-strength steel fibers. It offers superior durability, ductility, workability, and mechanical performance, effectively mitigating many of the limitations associated with conventional concrete [6,7]. At the same time, UHPC offers excellent compressive strength and good tensile toughness [23]. To date, extensive research has been conducted on UHPC structural applications. These include composite beams [24–26], novel reinforced components [21,23], and columns [27–29]. Studies have also focused on structural repair and strengthening [30–32]. Furthermore, investigations have covered its bond behavior with CFRP bars [4], GFRP bars [33,34], and conventional steel rebars [35–37]. UHPC enables efficient utilization of the tensile capacity of reinforcing bars; owing to its excellent bond strength, it can fully mobilize the tensile strength of steel reinforcement even with relatively short bond lengths [36]. Furthermore, the negative Poisson's ratio effect of NPR bars under tension generates greater radial compressive forces at the concrete interface, transforming what was initially passive interface friction into active compression. The exceptional shear strength and toughness of UHPC are well-suited to withstand and transfer the localized high stresses induced by NPR bars, effectively preventing premature splitting failure of the matrix. Consequently, the synergistic combination of UHPC and NPR reinforcement holds considerable promise. Numerous studies have recently investigated the bond performance of NPR-UHPC systems.

Lu et al. [17] reported that the ultimate bond strength of NPR bars in UHPC is 21% higher than that of HRB400 bars, though slightly lower than that of HRB635 bars, and systematically identified three typical failure modes. Xu et al. [16], through eccentric pullout tests, further confirmed the superior bond performance of NPR bars over HRB400 bars, while also identifying a significant negative effect of pre-strain: when pre-strain reached 22.0%, bond strength decreased by 17.01%. In addition, to address the underestimation of bond strength by existing physical models for this class of materials, Xu et al. [7] developed an artificial neural network model capable of predicting bond performance with an R^2 value exceeding 0.9, offering improved accuracy.

In light of the preceding observations, the empirical landscape regarding the interfacial bond performance between Negative Poisson's Ratio (NPR) steel and Ultra-High Performance Concrete (UHPC) remains conspicuously sparse. Prevailing scholarship has historically focused its scrutiny upon conventional deformed and helically ribbed variants of NPR reinforcement. Consequently, a profound investigative void persists concerning the interaction of smooth NPR bars and multi-wire strands within the UHPC matrix—a deficiency that leaves the governing internal bond mechanisms and constitutive models largely unexplored. Therefore, the present study addresses this gap by investigating the bond behavior between these distinct types of NPR reinforcement and UHPC. The effects of bond length and bar diameter were examined, and differences in failure modes among the various reinforcement types embedded in UHPC were analyzed. The characteristics of the bond-slip curves throughout the entire loading process were evaluated, and comparisons were made with the performance observed in normal concrete (NC). Based on these analyses and the identified influencing factors, predictive models for bond performance were developed through fitting, and empirical models were established.

2 Experimental Programs

2.1 Raw Materials

Three types of NPR reinforcement were employed in the tests: smooth bars, spiral-ribbed bars, and steel strands. The smooth NPR bars had a diameter of 9.6 mm; the spiral-ribbed NPR bars had a diameter of 18 mm; and the NPR steel strands had diameters of 15.2 and 21.6 mm. The physical appearance of the NPR reinforcement is shown in Fig. 1.

Figure 1: NPR tendons with different surface characteristics.

Tensile tests were conducted on the four types of NPR reinforcement in accordance with the standard GB/T 228.1-2010 [38]. The tensile stress–strain curves are presented in Fig. 2. It can be observed that all three types of NPR reinforcement exhibited distinct yield points during tensile loading. The curve trends of the NPR steel strands and spiral-ribbed NPR bars were similar, whereas the smooth NPR bars demonstrated substantially higher elongation than the other two types. The test results are summarized in Table 2. Furthermore, only slight necking was observed in the cross-sections of all NPR reinforcement types after fracture, reflecting the negative Poisson's ratio effect.

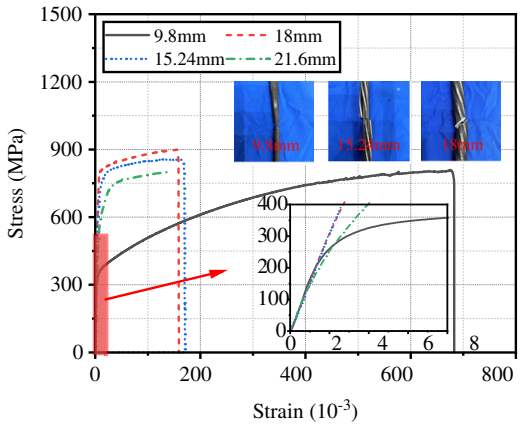

Figure 2: Strain-stress of NPR rebar.

Table 2: Test result of NPR rebar.

Types	Diameter (mm)	Yield Strength (MPa)	Ultimate Strength (MPa)	Elongation at Break (%)	Modulus of Elasticity (GPa)
Bare round rebar	9.6	362	806	51.2	150
Spiral ribbed rebar	18	808	897	20.8	147
Steel strand	15.24	784	854	19.9	154
	21.6	773	844	20.1	141

The UHPC mixture incorporated P.O. 52.5 Portland cement, Class I fly ash, silica fume with a particle size of 7000 mesh, quartz sand with a particle size range of 80–120 mesh, and copper-coated steel fibers with a diameter of 0.2 mm and a length of 13 mm. The properties of the steel fibers are listed in Table 3. In addition, a high-performance polycarboxylate superplasticizer was added during mixing to improve the flowability of the concrete.

Table 3: Properties of steel fibers.

Types	Length (mm)	Diameter (mm)	Aspect Ratio	Density (g/cm^3)	Tensile Strength (MPa)	Modulus of Elasticity (GPa)
Steel fiber	13	0.2	65	7.8	2850	210

2.2 Specimen Mix Proportion and Fabrication

2.2.1 Mix Proportion Design

The mix proportion of UHPC is provided in Table 4. The mechanical properties of the concrete were tested in accordance with the standard GB/T 50080-2016 [39], and the results are summarized in Table 5. The test results indicated that the 28-day compressive strength and splitting tensile strength of the concrete reached 186.6 and 14.9 MPa, respectively.

Table 4: Specimen ratio.

Mix.	Raw Material (kg/m^3)						
	Cement	FA	Silica Fume	Quartz Sand	Steel Fiber	Water	Water Reducer
UPHC	630	135	135	900	157	162	18

Table 5: Basic performance.

Mix.	Cubic Compressive Strength (MPa)		Splitting Tensile Strength (MPa)		Axial Compressive Strength (MPa)	Modulus of Elasticity (GPa)
	7-Days	28-Days	7-Days	28-Days	28-Days	
UPHC	89.33	128.62	10.71	14.90	97.67	42.31

2.2.2 Test Groups

The test groups are presented in Table 6. The specimen ID is defined as follows: 'UHPC' denotes the concrete type, 'R' represents the bar diameter, 'D' indicates the bond length, and 'T' specifies the type of NPR reinforcement. Specifically, T1, T2, and T3 correspond to smooth NPR bars, spiral-ribbed NPR bars, and NPR steel strands, respectively.

2.2.3 Specimen Fabrication

The bonded segment was positioned at the center of a standard 150 mm cubic concrete specimen, with bond lengths of 3 times the bar diameter (3d) and 5 times the bar diameter (5d). For the unbonded regions, PVC pipes were used to encase the reinforcement, secured with foam tape to seal the pipe ends. This

arrangement was intended to eliminate stress concentration effects at both the loaded and free ends and to prevent the ingress of cement paste. The mold configuration is detailed in Fig. 3.

Table 6: Test specimen group.

Specimen ID	Reinforcing Bar Diameter (mm)	Bond Length (mm)	NPR Type	Number of Components
UHPC-R9.6D3T1	9.6	28.8	Bare round rebar	3
UHPC-R9.6D5T1	9.6	48	Bare round rebar	3
UHPC-R18D3T2	18	54	Spiral ribbed rebar	3
UHPC-R18D5T2	18	90	Spiral ribbed rebar	3
UHPC-R15.24D3T3	15.24	45.72	Steel strand	3
UHPC-R15.24D5T3	15.24	76.2	Steel strand	3
UHPC-R21.6D3T3	21.6	65.4	Steel strand	3
UHPC-R21.6D5T3	21.6	109	Steel strand	3

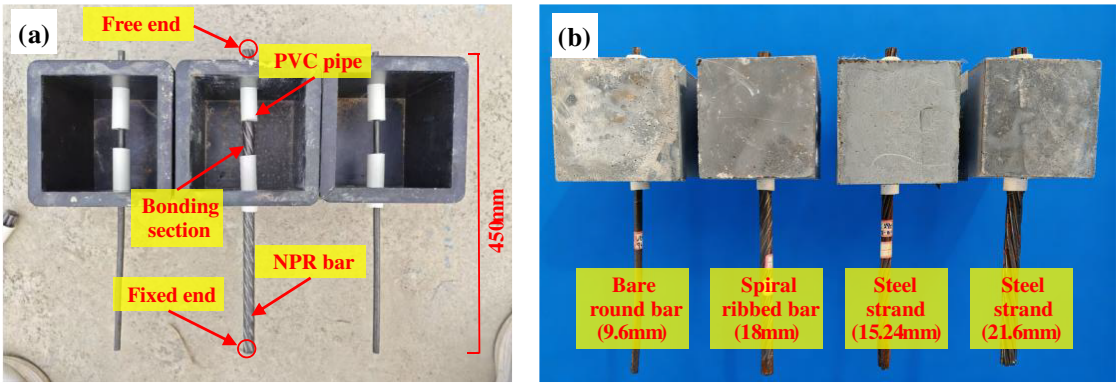

Figure 3: Pull-out specimen: (**a**) mold; (**b**) specimens.

During casting, the reinforcement bars were first placed horizontally into pre-drilled holes in the mold. The concrete mixture was then prepared. For UHPC, the cement, silica fume, fly ash, and quartz sand were dry-mixed for 3 min. Subsequently, mixing water and superplasticizer were added and wet-mixed for 5 min. Finally, once the matrix paste exhibited adequate flowability, the steel fibers were uniformly dispersed and mixed in, after which the mixture was discharged into the molds.

2.3 Test Method

Center pullout tests were conducted using a universal testing machine. The test setup comprised a suspended steel cage configured as a hanging basket, with a hemispherical hinge plate positioned on the bearing plate to ensure that the reinforcement remained aligned with the center of the grip throughout the pullout process, thereby avoiding eccentric loading. During loading, the testing machine displaced the steel cage and concrete specimen upward, inducing relative pullout displacement of the reinforcement clamped at the lower end. The test setup is shown in Fig. 4.

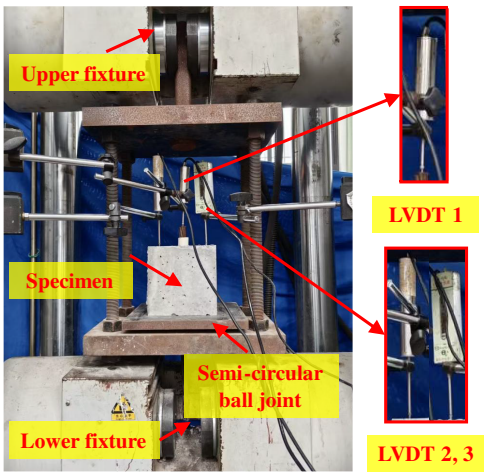

Figure 4: Setup of pull-out test.

Three electronic displacement transducers were employed: displacement transducer No. 1 (range: 30 mm) was installed at the free end of the reinforcement to monitor bar slip; Displacement transducers No. 2 and No. 3 (range: 50 mm) were symmetrically placed on the top surface of the concrete, and their average value was taken to eliminate displacement deviations arising from the concrete itself. The loading procedure followed the standard GB/T 50152-2012 [40], with an initial loading rate of 0.3 mm/min. Owing to the excellent ductility of NPR reinforcement, after the load reached its ultimate value, the loading rate was adjusted to 1 mm/min until specimen failure.

3 Test Results

Based on the characteristics of the bond-slip data, the slip stages of the smooth NPR bars and NPR steel strands were divided into Bond I and Bond II. To facilitate a more in-depth analysis of the pullout behavior of NPR reinforcement, the following discussion incorporates experimental observations and data from previous studies conducted by our research group on NPR reinforcement embedded in normal concrete (NC) for comparison. The test results and comparative data are summarized in Table 7, where each value represents the average of three replicate tests.

Table 7: Test result of bond stress and failure mode.

Specimen ID	Compressive Strength (MPa)	Bond Stress I (MPa)	Bond Stress II (MPa)	Bond Slip I (mm)	Bond Slip II (mm)	Failure Mode
UHPC-R9.6D3T1	128.62	12.29	11.46	0.82	13.18	P
UHPC-R9.6D5T1		11.55	10.88	1.28	14.18	P
UHPC-R18D3T2		35.18	N	3.96	N	SP
UHPC-R18D5T2		30.58	N	4.42	N	SP
UHPC-R15.24D3T3		7.16	9.76	0.88	16.53	P
UHPC-R15.24D5T3		5.49	7.95	1.28	18.65	P
UHPC-R21.6D3T3		4.68	6.84	1.10	49.25	P
UHPC-R21.6D5T3		3.70	5.29	1.67	64.34	SP

(Continued)

Table 7 (continued)

Specimen ID	Compressive Strength (MPa)	Bond Stress I (MPa)	Bond Stress II (MPa)	Bond Slip I (mm)	Bond Slip II (mm)	Failure Mode
NC-R9.6D3T1	51.42	1.81	4.73	0.39	42.15	P
NC-R9.6D5T1		2.70	4.83	0.36	51.63	P
NC-R18D3T2		21.61	N	4.64	N	P
NC-R18D5T2		18.81	N	3.51	N	S
NC-R15.24D3T3		4.72	7.16	0.27	35.32	P
NC-R15.24D5T3		3.14	5.26	0.20	57.56	P
NC-R21.6D3T3		2.14	6.08	0.30	60.50	SP
NC-R21.6D5T3		1.64	2.79	0.37	35.6	SP

3.1 Failure Modes

Observation of the failed specimens revealed that, for the UHPC matrix, the pullout process predominantly resulted in pullout failure for all types of NPR reinforcement, with a minor occurrence of splitting-pullout failure (specifically for R18-T2).

3.1.1 Smooth NPR Bars

The failure mode of the smooth NPR bars is illustrated in Fig. 5. Owing to the relatively smooth surface of these bars, the bond resistance primarily relied on interfacial chemical adhesion and friction, with no effective mechanical interlocking. Consequently, during pullout, the smooth NPR bar-UHPC specimens (UHPC-R9.6D3T1/D5T1) exhibited typical pullout failure. In this failure mode, the concrete matrix remained intact with no visible cracks; however, scratches resulting from friction and concrete powder were observed on the bar surface after pullout. Compared with smooth NPR bar-NC specimens, the failure mode was consistent, also characterized by pullout failure.

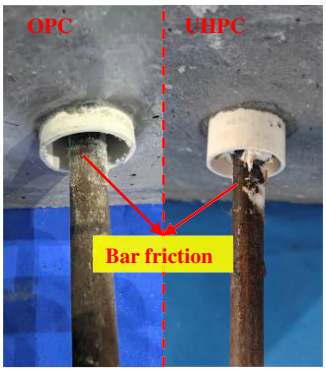

Figure 5: Failure mode of smooth NPR-UHPC and NPR-NC.

3.1.2 Spiral-Ribbed NPR Bars

The failure mode of the spiral-ribbed NPR bars is shown in Fig. 6. For specimens with a short bond length (3d), pullout failure occurred. In this case, the lateral confinement provided by the concrete was sufficient to resist the radial stresses induced by shearing at the rib-concrete interface; the matrix surface remained essentially crack-free, although fine scratches and concrete powder were evident on the bar surface.

However, as the bond length increased to 5d, the pullout load increased substantially, and the shear stress at the rib–concrete interface intensified, leading to splitting of the UHPC matrix.

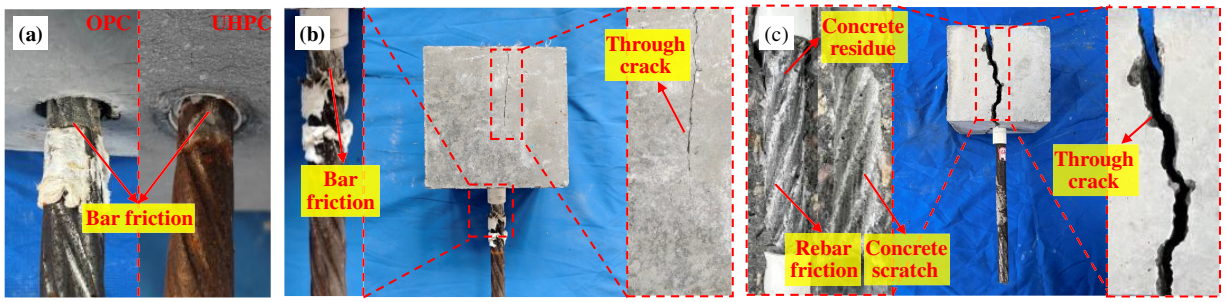

Figure 6: Failure mode of spiral-ribbed NPR-UHPC: (**a**) Pull-out failure; (**b**) Splitting pull-out failure; (**c**) Splitting failure.

Despite the occurrence of cracks, the steel fibers within the UHPC bridged the crack faces, restraining crack propagation and demonstrating the material's high tensile strength, thereby effectively inhibiting further splitting of the matrix. Accordingly, for the 5d bond-length groups, the failure mode was splitting-pullout failure. Although through-thickness cracks developed in the matrix, the two halves of the concrete remained interconnected due to fiber bridging, and the bar ultimately failed by slippage, reflecting excellent ductility. In the NC groups, pullout failure was also observed for a bond length of 3d. For a bond length of 5d, however, the absence of steel fibers in the ordinary Portland cement (OPC) matrix resulted in a lower interfacial tensile strength, which was insufficient to provide adequate confinement to resist the propagation of radial cracks, ultimately leading to brittle splitting failure.

3.1.3 NPR Steel Strands

The failure mode of the NPR steel strands is also presented in Fig. 7. NPR steel strands are manufactured using a helical winding process, and during pullout they typically exhibit a "rotational pullout" pattern along the concrete imprint [41], accompanied by a pronounced "strand expansion" effect. In the UHPC groups, all strand specimens failed in pullout mode. Owing to the extremely high compactness and strength of the UHPC matrix, the radial stresses generated by strand rotation and expansion were effectively confined, providing sufficient restraint to prevent the formation of through-going splitting planes. Examination of the pulled-out strand surfaces revealed fine scratches and strand expansion for both diameters. This phenomenon was more pronounced for the 21.6 mm diameter strand group, which exhibited a greater degree of overall untwisting and expansion. In the NC groups, the smaller-diameter strands also failed by pullout. However, for the large-diameter NPR strand specimens (R = 21.6 mm), the expansion pressure generated during pullout was excessive, and the tensile strength of the NC matrix was insufficient to provide the necessary confinement to resist strand deformation. Consequently, a splitting-pullout failure occurred during the pullout process. In this case, the strand exhibited significant rotation and untwisting, accompanied by crushing failure of the interlocking teeth in the concrete matrix.

3.2 Bond-Slip Curves

Typical bond-slip curves were selected from each test group. Based on the combined data from three replicate tests, the bond-slip curves were constructed for the smooth NPR bars, spiral-ribbed NPR bars, and NPR steel strands. The average bond stress τ between the reinforcement and concrete during the loading stage was calculated using the following equation:

$$\tau = \frac{F}{\pi d l_a} \tag{1}$$

where F is the applied load on the bar (N), d is the bar diameter (mm), and l_a is the anchorage length (mm).

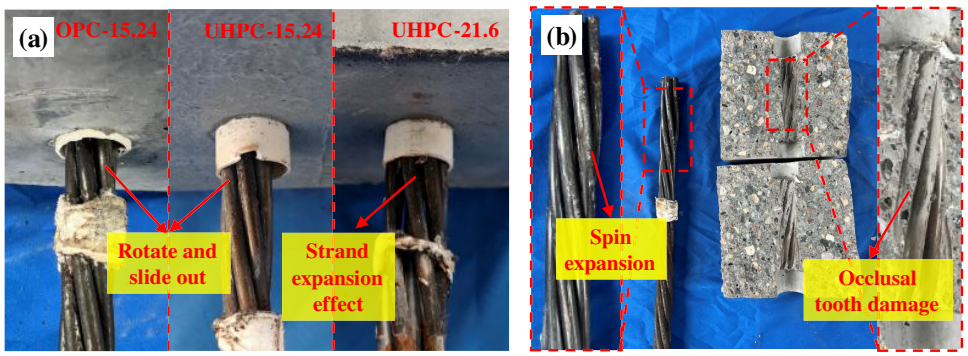

Figure 7: Failure mode of NPR steel strands—UHPC: (**a**) Pull-out failure; (**b**) Splitting pull-out failure.

The relative slip corresponding to each load level comprises both the slip of the concrete and the deformation of the reinforcement within the bonded length. The average slip between the reinforcement and concrete is given by:

$$s = s_c - s_r \tag{2}$$

where s_c is the slip of the concrete (mm), obtained as the average value measured by displacement transducers No. 2 and No. 3 mounted on the concrete top surface; and s_r is the deformation of the reinforcement within the anchorage length (mm), recorded by displacement transducer No. 1 at the free end of the bar.

3.2.1 Smooth NPR Bars

The bond-slip curves for the smooth NPR bars are presented in Fig. 8. All specimens in this group exhibited pullout failure. For the UHPC matrix groups, the curves can be characterized by four stages: a micro-slip stage (slip of approximately 1–2 mm), a slip stage (slip of approximately 2–5 mm), a friction-expansion stage (slip of approximately 10–15 mm), and a descending stage. In the micro-slip stage, bond resistance is primarily provided by chemical adhesion at the concrete–bar interface, and the curve exhibits a linear increase. During this stage, only minor slip occurs; upon reaching the first ultimate bond strength, the chemical adhesion breaks down. Upon entering the slip stage, a sudden drop appears in the bond–slip curve, as the interfacial resistance mechanism transitions from chemical adhesion to friction, leading to a rapid increase in slip. Subsequently, the process enters the friction expansion phase. Unlike conventional steel bars, which exhibit radial contraction due to the positive Poisson's ratio effect when subjected to tensile stress, NPR reinforcements experience a slight expansion effect under axial tensile stress. Due to the high radial confinement stiffness of the UHPC matrix, the deformations resulting from this expansion are effectively restrained and converted into normal pressure at the interface. Therefore, during this process, the NPR effect generates greater interface friction, leading to a resurgence in stress. The bond strength increases with the slip, and when the slip reaches a certain level, the friction force reaches its limit, marking the attainment of Ultimate Strength II. In the descending stage, continued wear smooths both the bar surface and the surrounding concrete, causing a rapid reduction in bond stress until complete pullout occurs.

The NC groups failed by pullout but showed clear differences from UHPC. NC's chemical adhesion was much lower than UHPC's in the micro-slip stage. In the friction-expansion stage, aggregate interlocking in

NC gave greater slip and higher second ultimate bond strength. Smooth NPR bars have very different bond-slip behavior from conventional smooth bars. For conventional NPR bars, bond stress usually drops a little after the peak and then stays at a quite high residual level during pullout [42]. The negative Poisson's ratio effect of NPR material gives higher residual bond strength. For UHPC groups, the curve in the residual stage goes up first then down. For NC, it shows an irregular slow increase.

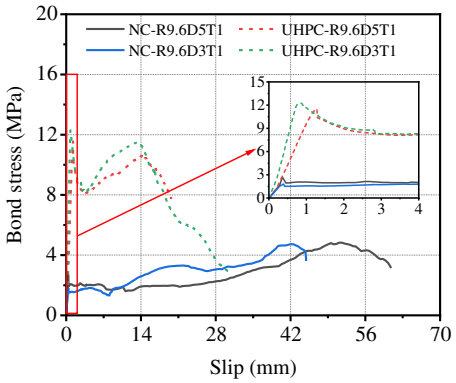

Figure 8: Bond-slip curves of smooth NPR bar.

3.2.2 Spiral-Ribbed NPR Bars

Fig. 9 shows the bond-slip curves for spiral ribbed NPR bars. Overall, the pullout failure curves of the helical rib NPR reinforcements exhibit similar shapes and show no significant differences compared to the pullout curves of ordinary helical ribs and ordinary ribbed reinforcements [43,44]. For the UHPC matrix specimens with a bond length of 3d, the bond–slip curves can be divided into four stages: a micro-slip stage (1–3 mm), a slip stage (5–7 mm), a descending stage (8–16 mm), and a residual stage.

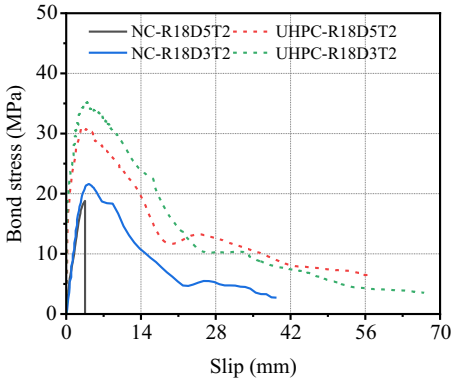

Figure 9: Bond-slip curves of spiral-ribbed NPR bars.

In the micro-slip stage, bond resistance is primarily governed by chemical adhesion at the interface, and the curve rises steeply with a high initial slope. As the slip stage commences, the bond mechanism gradually shifts from chemical adhesion to friction and mechanical interlocking between the ribs and the concrete. During this stage, the rate of bond stress increase slows, and the curve assumes a more gradual, arc-like shape. As the pullout load continues to increase, the compressive stress exerted on the concrete interlocking keys reaches its maximum, and the curve attains the ultimate bond strength. Upon entering the descending stage, the concrete keys are progressively crushed under compression, leading to a gradual loss of mechanical

interlock and a rapid decline in bond stress. In the residual stage, the NPR bar's negative Poisson's ratio effect stops the bar diameter from shrinking much. Residual compressive stress from partly flattened concrete ribs and friction from crushed concrete particles at the interface give a small bond stress recovery. Bond failure happens when the concrete ribs are fully crushed.

UHPC specimens with 5d bond length had bond-slip curves like the 3d ones. Splitting grew slowly, not all at once. The curves had four stages, and the first two were the same as 3d. After the slip stage, the curve hit the ultimate bond strength and then went into a cracking and descending stage. Bond resistance still came from concrete ribs pressing on the bar, but the longer bond length raised the interfacial loads. The concrete could not take the rib pressure, reached its tensile limit, and started fine cracks. Steel fibers in UHPC slowed crack growth. In the residual stage, fiber bridging kept the concrete interface together, delayed big cracks, and gave a small second rise in bond stress. When internal cracks joined and spread through the matrix, bond stress dropped again and cracks ran through the thickness.

NPR spiral ribbed bar and NC specimens with 3d bond length acted like UHPC 3d ones and failed by pullout. For 5d bond length, the weaker NC matrix caused splitting failure. The curves had three stages. The first two matched UHPC groups, and the third was splitting failure. NC matrix had lower tensile strength and no steel fibers. With high rib pressure, the concrete could not hold the bar, reached its tensile limit, and split. This was brittle failure.

3.2.3 NPR Steel Strands

Fig. 10 shows bond-slip curves for NPR steel strands. The pullout process had a small first peak, then a slight drop, and then went up again. This is different from conventional steel strands, which have a stable or slowly dropping curve after the peak [45]. For UHPC groups with 15.24 mm strands, the bond-slip curves were similar and had four stages: micro-slip (0–2 mm), slip (2–6 mm), strand expansion (6–18 mm), and residual.

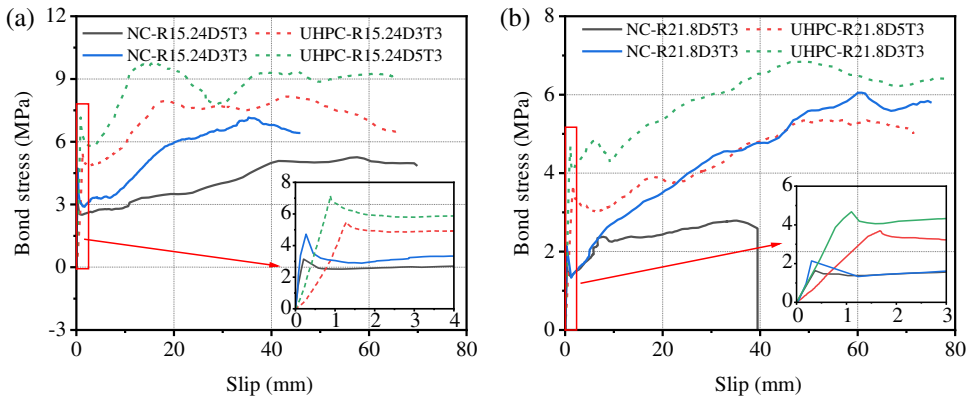

Figure 10: Bond-slip curves of NPR steel strands: (**a**) R15.24T3; (**b**) R21.6T3.

The micro-slip and slip stages had the same features as those seen on smooth NPR bars. In the strand expansion stage, the pullout force gradually became compressive stress at the interface of the helical strand surface and the matching concrete mark. At the same time, each wire in the strand started to untwist and stretch under the pullout load, with no obvious necking. This process made the strand's total diameter bigger little by little. It put more radial pressure on the concrete around, and made the frictional resistance even stronger.

When the helical marks in the concrete broke, the specimen hit its ultimate bond strength. Then the residual stage started. During this stage, the bonding force primarily arises from the friction between the unpolished helical patterns within the concrete and the radial expansion of the steel strand wires. As the steel strand rotates and is pulled out, the untwisting tendency of individual wires and the radial displacement induced by the NPR effect enhance the anchoring interaction at the interface between UHPC and the reinforcement. This leads to an increase in normal pressure at the interface, gradually elevating the bond stress. Consequently, the slip curve exhibits irregular fluctuations until the steel strand is completely extracted. The UHPC group with 21.6 mm diameter strands had a more obvious strand expansion effect because the strands were thicker. Compared with the 15.24 mm group, the slip range in the strand expansion stage reached 6–60 mm. This shows the thicker strand put more radial pressure when being pulled out.

For NPR steel strand-NC specimens, the micro-slip and slip stages were much shorter. Slip ranges were 0–0.5 and 1–2 mm. For NC with 15.24 mm strands, the strand expansion stage had a slip range of 2–40 mm. For NC with 21.6 mm strands and 3d bond length, the strand expansion stage also had a slip range of 2–60 mm. The stage characteristics were like those of UHPC groups. But for NC with 21.6 mm strands and 5d bond length, splitting failure happened. The bond-slip curve had three stages. The first two were the same as before, and the third was a strand expansion–splitting stage. NC matrix had lower tensile strength than UHPC. It could not take the expansion pressure from the large strand under long bond length. When the expansion force went over the NC matrix's tensile strength, the concrete split. Bond stress dropped suddenly, and failure was catastrophic.

3.3 Influence of Different Factors on Bond Performance

3.3.1 NPR Reinforcement Type

Fig. 11 shows how NPR bar type and bond length affect bond-slip performance. Of smooth NPR bars, spiral ribbed NPR bars, and NPR steel strands (15.24 and 21.6 mm), spiral ribbed bars had the highest bond strength. This is because their continuous helical ribs give strong mechanical interlock during pullout. Smooth NPR bars had middle bond strength. They have no ribs, but high chemical adhesion with the strong UHPC matrix still gave good bond resistance. NPR steel strands had the lowest bond performance. This is mostly from the strand expansion effect during pullout, which caused instability and limited the use of chemical adhesion and rib shear resistance at the interface.

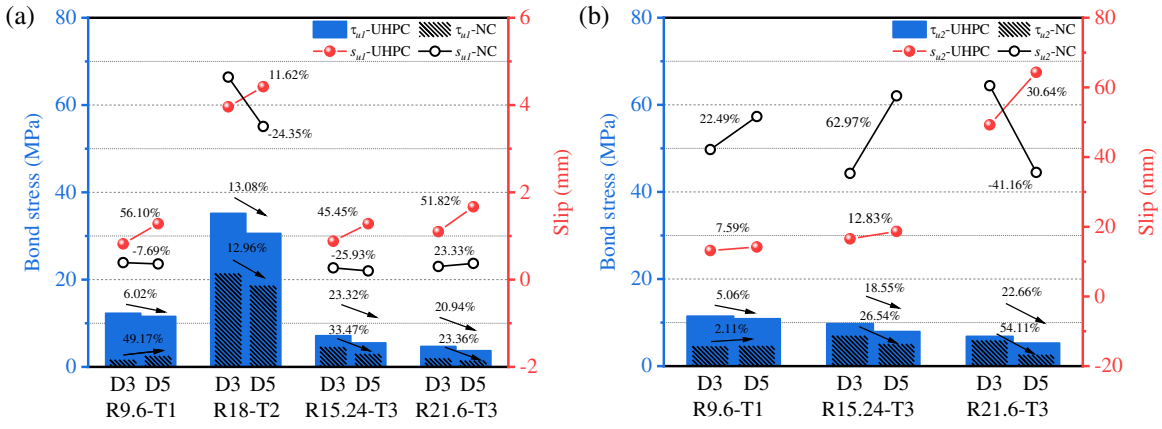

Figure 11: Effects of NPR tendon type and bond length on bond-slip behavior: (**a**) Stage I; (**b**) Stage II.

As for ultimate slip, smooth NPR bars had a slip of 30–60 mm at ultimate bond strength. This is much more than the usual 10–15 mm of ordinary smooth steel bars set in concrete [46]. On the other hand, spiral ribbed NPR bars had the smallest ultimate slip, usually only 3–5 mm. Besides, the residual slip of ordinary spiral ribbed bars usually drops to the lowest at about 20 mm. This is far less than the 40–70 mm of NPR spiral ribbed bars. What's more, NPR steel strands had the biggest ultimate slip, hitting 40–70 mm [44]. Among these strands, the 21.6 mm one slipped more in the second stage than the 15.24 mm one. Both of them slipped more than smooth NPR bars and spiral ribbed bars in the first stage. Ordinary steel strands usually have an ultimate slip of 3–20 mm [45]. But NPR steel strands had an ultimate slip of 30–70 mm when pulled out under tension.

Compared with the NC groups, the order of bond strength was different because the matrix properties were not the same. In the NC groups, smooth NPR bars had the lowest ultimate bond strength, then came the steel strands. Spiral ribbed bars had the highest ultimate strength again. This may be because the NC matrix is not very strong. It can only provide weak chemical adhesion, so smooth bars contribute very little to the bond. Also, the ultimate slip performance in the first and second stages did not follow the same rule.

3.3.2 Bond Length

Fig. 11 compares the bond performance with different bond lengths. People all know that making the bond length longer will lower the average bond strength [3,47–49]. In the UHPC matrix groups, both the first and second stage bond strengths went down when the bond length got longer. When the bond length grew from 3d to 5d, the bond strength of smooth bar, spiral ribbed bar and steel strand groups dropped by 5.54%, 13.08% and 21.37% on average. This is because the bond stress is not evenly distributed at all along the longer embedded parts [44]. On the contrary, the ultimate slip of all groups went up when the bond length got longer. When the bond length grew from 3d to 5d, the ultimate slip of smooth bar, spiral ribbed bar and steel strand groups rose by 31.85%, 11.62% and 35.19% on average. This shows that longer bond length helps to improve the slip ability.

In the NC groups, all groups except the smooth NPR bar group had the same trend as the UHPC groups. That is, the ultimate strength went down when the bond length got longer. But the smooth NPR bar group was the opposite. Both the first and second stage bond strengths went up when the bond length got longer. This may be because there is coarse aggregate in the NC matrix. It makes the confinement around the smooth bar stronger, so the bond resistance gets better. As for ultimate slip, the spiral ribbed bar group and the 21.6 mm steel strand group had smaller ultimate slip when the bond length grew from 3d to 5d. This is because the failure mode changes from pullout to splitting when the embedded part is longer. The concrete splits early before it reaches the maximum slip. The other groups had the same trend as the UHPC groups. Their ultimate slip went up when the bond length got longer.

3.3.3 NPR Reinforcement Diameter

Fig. 12 analyzes the bond performance of NPR steel strands with 15.24 and 21.6 mm diameters. People all know that making the bar diameter bigger usually lowers the bond strength [3]. In the UHPC groups, when the strand diameter grew from 15.24 to 21.6 mm, the ultimate bond strength dropped a lot, by 32.32% on average. In the first stage, the average drop was 34.64%. In the second stage, the drops were 15.08% and 46.96%. This trend is the same as the pullout performance of ordinary steel strands [50]. At the same time, the ultimate slip of the strands went up a lot, by 124.6% on average in both the first and second stages. Compared with the NC groups, all specimens had the same trend except those in the second stage with a 5d bond length. For the 21.6 mm strands set in NC, the failure mode changes from pullout to splitting when the bond length grows from 3d to 5d. This change makes the failure more brittle and sudden, so the ultimate slip gets smaller.

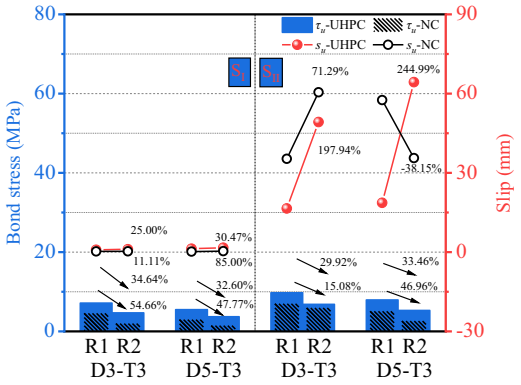

Figure 12: Effect of steel bar diameter on bond performance.

3.3.4 Concrete Type

The influence of concrete types on bond performance is illustrated in Fig. 13. Across all NPR reinforcement types, the UHPC matrix groups consistently exhibited superior bond performance compared to the NC groups. This advantage is primarily attributable to the high compressive strength of UHPC and the excellent tensile properties imparted by the incorporated steel fibers, which together provide enhanced confinement during pullout and effectively resist the applied pullout load. In contrast, the NC groups exhibited an average reduction in ultimate bond strength of 47.07% relative to the UHPC groups. Specifically, during the first stage, the ultimate bond strength of the UHPC matrix groups was on average 55.68% higher than that of the NC groups. Regarding ultimate slip, during the first stage, the UHPC matrix exhibited greater ultimate slip in most groups, with the exceptions of the R1-D5 and R2-D3 groups. During the second stage, however, the ultimate slip of UHPC-embedded specimens was generally lower than that of NC-embedded specimens, except in the R4-D5 group, where splitting failure occurred in the NC specimen and resulted in lower ultimate slip than its UHPC counterpart. These observations suggest that the UHPC matrix exerts a stage-dependent influence on the pullout behavior of NPR reinforcement: while its higher strength and toughness enhance bond resistance, they may concurrently constrain the development of ultimate slip.

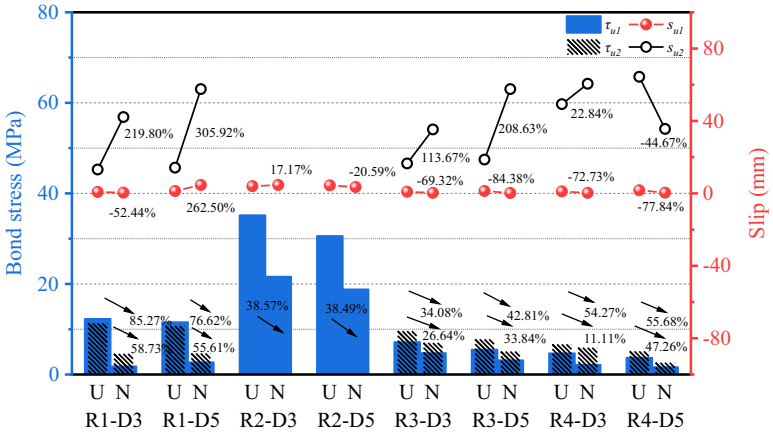

Figure 13: Effect of concrete type on bond performance.

4 Theoretical Models

4.1 Ultimate Bond Strength

(1) Smooth NPR bars:

Since the bond strength reaches its maximum during the first stage, only the ultimate bond strength (τ_{u1}) and the corresponding slip (s_{u1}) in this stage are fitted. The effects of concrete compressive strength (f_{cu}) and cover thickness (c) on the ultimate bond strength are considered. The fitting formula is given as follows:

$$\tau_{u1} = \left(0.49\frac{d}{l_a} + 0.92\right)\sqrt{f_{cu}} \tag{3}$$

(2) NPR steel strands:

Referring to the model for conventional steel strands embedded in concrete proposed by Xiong et al. [51], the ultimate bond strength and the corresponding slip of the NPR steel strands in this study are fitted. The model exhibits good fitting accuracy and is expressed as:

$$\tau_{u1} = \left[0.000642\left(92.59\frac{c}{d} + 7.53\right)\right]\left(3.7\frac{d}{l_a} - 0.0068\right)\left(0.28\frac{l_a}{d} + 1.06\right)\sqrt{f_{cu}} \tag{4}$$

For the second stage:

$$\tau_{u2} = \left[0.002084\left(36.58\frac{c}{d} + 7.53\right)\right]\left(3.7\frac{d}{l_a} + 0.03\right)\left(0.31\frac{l_a}{d} + 1.03\right)\sqrt{f_{cu}} \tag{5}$$

An empirical model for τ_{u2} based on τ_{u1} is also established:

$$\tau_{u2} = 1.28\tau_{u1} + 0.74 \tag{6}$$

(3) Spiral-ribbed NPR bars:

Following the fitting approach proposed by Lu et al. [17] for spiral-ribbed reinforcement, the ultimate bond strength of the spiral-ribbed NPR bars is expressed as:

$$\tau_{u1} = 0.020\left(\frac{E_s}{E_{sx}}\right)^{0.8}\left(12.10 + \frac{c}{d}\right)\left(0.27 + \frac{d}{L_a}\right)\left(14.73 + \lambda_f\right)\sqrt{f_{cu}} \tag{7}$$

where λ_f is the fiber characteristic value (calculated as $\lambda_f = V_f \times L_f/d_f$); f_{cu} is the cubic compressive strength of UHPC (in MPa); E_s is the secant modulus of the spiral-ribbed NPR bar at a strain of 0.2%; and E_{sx} is the standard elastic modulus of the spiral-ribbed NPR bar. All these material parameters are obtained from Section 2.1.

(4) Comprehensive model:

To enable a more generalized prediction of the bond–slip behavior of various NPR reinforcement types, a comprehensive model incorporating an NPR reinforcement coefficient (α) is developed. The model accounts for the effects of bar diameter, concrete cover thickness, concrete strength, and bond length, and is expressed as:

$$\tau_{u1} = \left(\Delta_{T,\tau} + 0.1299\frac{c}{d} + 1.3210\frac{d}{L_a}\right)\sqrt{f_{cu}} \tag{8}$$

The value of $\Delta_{T,\tau}$ is taken as −0.2512 for smooth NPR bars, 2.0706 for spiral-ribbed NPR bars, and −0.3689 for NPR steel strands.

4.2 Ultimate Slip

(1) Smooth NPR bars:

The ultimate slip in the first stage (s_{u1}) is fitted considering only the influence of NPR bar diameter (d) and bond length (l_a):

$$0.23\frac{l_a}{d} + 0.13 \tag{9}$$

(2) NPR steel strands:

The ultimate slip model accounts for the interactive effects of $\frac{c}{d}$ and $\frac{l_a}{d}$. The fitting formulas are as follows:

$$s_{u1} = 0.0242\left(\frac{c}{d}\right) + 0.4593\left(\frac{l_a}{d}\right) - 0.0587\left(\frac{c}{d}\frac{l_a}{d}\right) + 0.1732 \tag{10}$$

For the second stage:

$$s_{u2} = -9.154\left(\frac{c}{d}\right) + 20.847\left(\frac{l_a}{d}\right) - 4.475\left(\frac{c}{d}\frac{l_a}{d}\right) + 53.824 \tag{11}$$

An empirical model for s_{u2} based on s_{u1} is also proposed:

$$s_{u2} = 17.935s_{u1} - 20.916\left(\frac{c}{d}\right) + 93.204 \tag{12}$$

(3) Spiral-ribbed NPR bars:

Considering the influence of $\frac{l_a}{d}$, the ultimate slip model is fitted as:

$$s_{u1} = 0.23\left(\frac{L_a}{d}\right) + 3.27 \tag{13}$$

(4) Comprehensive model:

The comprehensive model for ultimate slip is expressed as:

$$s_{u1} = \Delta_{T,s} - 0.0528\left(\frac{c}{d}\right) + 0.2388\left(\frac{L_a}{d}\right) \tag{14}$$

where $\Delta_{T,s}$ is the NPR reinforcement coefficient for slip, taken as 0.5050 for smooth NPR bars, 3.5450 for spiral-ribbed NPR bars, and 0.5360 for NPR steel strands.

4.3 Model Fitting Performance

The fitting performance of the proposed models is presented in Fig. 14. The validation results indicate that the theoretical models developed in this study achieve high predictive accuracy for the bond characteristic values of the three types of NPR reinforcement. Specifically, the ultimate strength models derived from the parametric approach provide good fits to the experimental data for both the smooth and spiral-ribbed NPR bars. For these two reinforcement types, the R^2 values of both the parametric and

empirical models consistently exceed 0.7. However, the first-stage model for the NPR steel strands exhibits relatively poor fitting performance, with an R^2 of only 0.6. With respect to ultimate slip, all model types-with the exception of that for the spiral-ribbed NPR bars-demonstrate satisfactory fitting capability, attaining R^2 values above 0.7. The ultimate slip model for the spiral-ribbed NPR bars yields a comparatively low R^2 of 0.6. Furthermore, the comprehensive model, which incorporates a reinforcement-type coefficient, effectively captures the bond characteristics of bars with different cross-sectional geometries. This proposed comprehensive model exhibits good fitting performance; its predictive accuracy remains largely comparable to that of the parametric models in most cases, with only marginal reductions observed in a few instances.

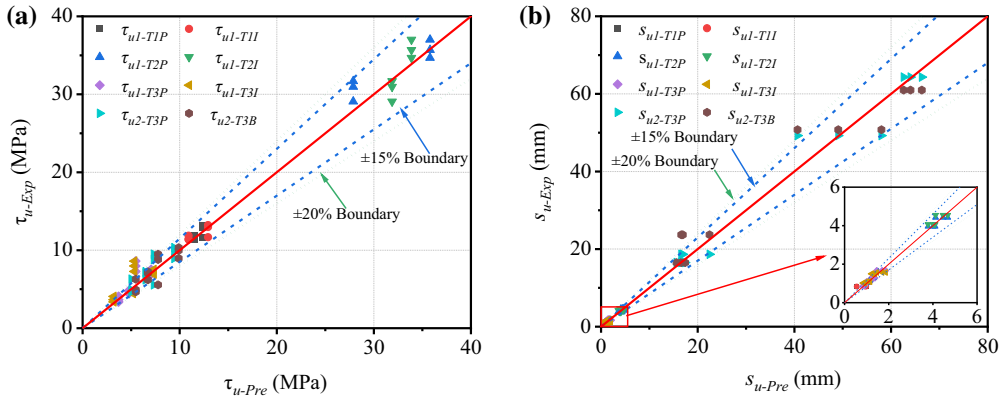

Figure 14: Goodness of fit of the model: (**a**) τ_u (**b**) s_u.

A comparison between the experimental and predicted values is illustrated in Fig. 14. The test results prove that the theoretical models we built are reliable enough to predict the bond performance of different NPR reinforcements set in UHPC. When we put the test data into the models for comparison and analysis, most data points are within the ±15% error range of the y = x reference line. Almost all points are within the ±20% error range. What's worth noting is that quite a few data points of NPR steel strands go beyond the ±20% error range. This may be because the strands are under complex stress during the whole pullout process. Plus the strand expansion effect, it's harder to predict the result accurately. Also, we need to note that the bond-slip performance of different NPR reinforcements in UHPC is affected by many factors. These include the production process of NPR bars, the fiber content and mix ratio of the UHPC matrix, and other things.

5 Conclusions

This study investigates the bonding performance of different types of Negative Poisson's Ratio (NPR) reinforcements using ultra-high performance concrete (UHPC) as the matrix. The key findings are as follows:

(1) The high compressive strength of UHPC and the bridging effect of fibers significantly enhance the lateral confinement of the reinforcements. As a result, the NPR reinforcements experience a transition from typical splitting failure in ordinary concrete to a more ductile pullout failure or splitting-pullout failure. Compared to ordinary concrete, the ultimate strength of UHPC increases the load-bearing capacity and ductility by 47.07%, resulting in greater structural reliability.

(2) The bond-slip curves reveal that for smooth NPR reinforcements, the bonding force is primarily governed by chemical adhesion, resulting in lower bonding strength. In contrast, the helical rib NPR reinforcements are dominated by mechanical interlocking, which leads to the highest bonding strength. The NPR steel strands, influenced by the expansion effect of their wires, display significant

residual stress and slip during their pullout process, providing advantages in energy-dissipating components.

(3) An increase in the diameter of NPR reinforcements or a decrease in bond length results in reduced ultimate strength and increased slip. For NPR steel strands, increasing the diameter leads to an average decrease in ultimate strength by 32.32% and an increase in ultimate slip by 124.6%. Among the three types of NPR reinforcements, helical rib reinforcements provide the highest mechanical interlocking strength, followed by smooth reinforcements, while the steel strands demonstrate the lowest ultimate strength due to their unstable pullout loading mechanism. Across all types of NPR reinforcements, bond length increases from 3d to 5d average by 26.22%.

(4) The bonding performance models for the three types of NPR reinforcements and UHPC were fitted using both parameter-based and empirical models. The fitting results were satisfactory, with most models achieving a correlation coefficient (R^2) greater than 0.7 and prediction errors maintained within ± 20%. By incorporating NPR reinforcement coefficients, a comprehensive model for the three types of NPR reinforcements was developed, which shows good overall fitting. This model can serve as a theoretical reference for the preliminary design of such composite structures.

6 Future Work

1. The models proposed in this study are primarily empirical; their accuracy may be compromised in practical applications due to variations in service conditions. Consequently, future research should conduct an in-depth analysis of the models' generalisability and optimise their scope of application to enhance their reliability and accuracy under a variety of complex service conditions.
2. Current bond tests have primarily focused on specimens with bond lengths of 3d and 5d, and have only investigated UHPC of a single strength grade. The range of bond lengths and UHPC strengths tested is relatively limited and is insufficient to fully reflect the bonding performance characteristics between various types of plain NPR bars, spiral-ribbed bars and steel strands and UHPC in actual engineering applications. In future research, tests should be conducted across a broader range of bond lengths, and analytical studies should be carried out on UHPC of different strength grades. By expanding the range of test parameters, the robustness and generalisability of the conclusions and models can be enhanced.

Acknowledgement: Not applicable.

Funding Statement: Science and Technology Projects of Xizang Autonomous Region, China (XZ202402ZD0003), Key Research and Development Program of Yunnan Province (202303AA080012), Natural Science Foundation of Fujian Province (2025J01371) and Fujian University of Technology (GY-Z220229 and GY-Z220228).

Author Contributions: The authors confirm contribution to the paper as follows: study conception and design: Qinfeng Pan and Xiang Liu; data collection: Hao Chen, Lin Pang and Chun Chieh Yip; analysis and interpretation of results: Xiang Liu, Hao Chen and Lin Pang; draft manuscript preparation: Qinfeng Pan and Wei Zhang. All authors reviewed and approved the final version of the manuscript.

Availability of Data and Materials: Data available on request from the authors. The data that support the findings of this study are available from the corresponding author.

Ethics Approval: Not applicable.

Conflicts of Interest: The authors declare no conflicts of interest.

References

1. Wang M, Wang Y, Zhang X, Chen G. Bond behavior and bond strength model for ribbed FRP bar in FRP-confined concrete. Constr Build Mater. 2024;449:138318. doi:10.1016/j.conbuildmat.2024.138318.
2. Zeng JJ, Liao J, Zhuge Y, Guo YC, Zhou JK, Huang ZH, et al. Bond behavior between GFRP bars and seawater sea-sand fiber-reinforced ultra-high strength concrete. Eng Struct. 2022;254(2):113787. doi:10.1016/j.engstruct.2021.113787.
3. Liu X, Chen H, Zhang W. Bond behavior of epoxy-coated reinforcement in FRP-confined seawater sea-sand geopolymer concrete. Case Stud Constr Mater. 2026;24:e05848. doi:10.1016/j.cscm.2026.e05848.
4. Yoo SJ, Hong SH, Yoon YS. Bonding behavior and prediction of helically ribbed CFRP bar embedded in ultra high-performance concrete (UHPC). Case Stud Constr Mater. 2023;19(2):e02253. doi:10.1016/j.cscm.2023.e02253.
5. He M, Ren S, Xu H, Luo S, Tao Z, Zhu C. Experimental study on the shear performance of quasi-NPR steel bolted rock joints. J Rock Mech Geotech Eng. 2023;15(2):350–62. doi:10.1016/j.jrmge.2022.03.011.
6. Shao SW, Shang HS, Feng HB, Wang WZ. Study on the mechanical properties of NPR steel bars and the bonding properties with marine concrete. Constr Build Mater. 2022;316(5):125721. doi:10.1016/j.conbuildmat.2021.125721.
7. Xu Z, Xu CZ, Rong XL, Wang JY, Ge PF. Bond performance and constitutive model of novel NPR rebar–UHPC system under monotonic loading. Case Stud Constr Mater. 2025;23(5):e05236. doi:10.1016/j.cscm.2025.e05236.
8. De Cooman BC, Estrin Y, Kim SK. Twinning-induced plasticity (TWIP) steels. Acta Mater. 2018;142:283–362. doi:10.1016/j.actamat.2017.06.046.
9. Xu S, Ruan D, Beynon JH, Rong Y. Dynamic tensile behaviour of TWIP steel under intermediate strain rate loading. Mater Sci Eng A. 2013;573:132–40. doi:10.1016/j.msea.2013.02.062.
10. Idrissi H, Renard K, Ryelandt L, Schryvers D, Jacques PJ. On the mechanism of twin formation in Fe–Mn–C TWIP steels. Acta Mater. 2010;58(7):2464–76. doi:10.1016/j.actamat.2009.12.032.
11. Yu WX, Liu BX, Cui XP, Dong YC, Zhang X, He JN, et al. Revealing extraordinary strength and toughness of multilayer TWIP/Maraging steels. Mater Sci Eng A. 2018;727(4):70–7. doi:10.1016/j.msea.2018.04.097.
12. Grässel O, Krüger L, Frommeyer G, Meyer LW. High strength Fe–Mn–(Al, Si) TRIP/TWIP steels development—properties—application. Int J Plast. 2000;16(10–11):1391–409. doi:10.1016/S0749-6419(00)00015-2.
13. Li X, Xue T, Sun Y, Wang P, Zhang L, Bu Y, et al. Experimental study of bonding properties of Negative Poisson's ratio (NPR) effect bars to concrete. Structures. 2025;73(2):108293. doi:10.1016/j.istruc.2025.108293.
14. Zhou J, Shang H, Chen Y, Fan L, Li Y, Liu H. Study on bond properties of corroded NPR (negative Poisson's ratio) steel bar embedded in marine concrete. Structures. 2023;57(10):105251. doi:10.1016/j.istruc.2023.105251.
15. Xiong X, Zhang Y, Liu J, He M. Bond behavior of concrete reinforced with high-strength and high-toughness steel bars. Constr Build Mater. 2023;370(12):130433. doi:10.1016/j.conbuildmat.2023.130433.
16. Xu Z, Xu CZ, Rong XL, Wang JY, Ma XY. Bond behavior and critical anchorage length prediction of novel negative Poisson's ratio bars embedded in ultra-high-performance concrete. Materials. 2025;18(13):3182. doi:10.3390/ma18133182.
17. Lu BL, Chang SY, Wang JY, Su BD, Liu KZ. Study on the bond properties of NPR steels and high-strength steels with ultra-high performance concrete. Constr Build Mater. 2025;466(9):140276. doi:10.1016/j.conbuildmat.2025.140276.
18. Gu JB, Wang JY, Lu W. An experimental assessment of ultra high performance concrete beam reinforced with negative Poisson's ratio (NPR) steel rebar. Constr Build Mater. 2022;327(3):127042. doi:10.1016/j.conbuildmat.2022.127042.
19. Long XC, Wang JY, Rong XL, Lu BL, Chen LB, Chen ZW. Cyclic performance of novel NPR steel-reinforced UHPC beams. J Build Eng. 2025;103(7):112181. doi:10.1016/j.jobe.2025.112181.
20. Zheng X, Tao Z, He M, Geng L. Investigation of the mechanical response and failure mode of high-ductility concrete (HDC) beams reinforced with negative Poisson's ratio (NPR) steel rebar. Constr Build Mater. 2025;475:141178. doi:10.1016/j.conbuildmat.2025.141178.
21. Zhang R, Tao Z, Xiong Y, He M. Experimental analysis and prediction of flexural performance in high-ductility UHTCC concrete beams reinforced with NPR materials. Structures. 2025;77(1):109084. doi:10.1016/j.istruc.2025.109084.

22. Lu BL, Wang JY, Rong XL, Chen LB, Chen ZW. Bond performance of novel NPR rebar-reinforced UHPC under cyclic loading. Constr Build Mater. 2025;474(7):140987. doi:10.1016/j.conbuildmat.2025.140987.
23. Zeng JJ, Sun HQ, Deng RB, Yan ZT, Zhuge Y. Bond performance between FRP bars and 3D-printed high-performance concrete. Structures. 2025;73(2):108377. doi:10.1016/j.istruc.2025.108377.
24. Li L, Wang X, Jin W, Lu B, Xiao G, Tang J. Experimental study on the structural performance of UHPC shell composite beam in the negative moment zone. Eng Struct. 2026;350(2):122027. doi:10.1016/j.engstruct.2025.122027.
25. Hu Y, Chen Y, Yao Y, Lin P, Wang J. Flexural behaviors of prestressed composite UHPC-NC beams with pre-tensioned and retard-tensioned tendons. Eng Struct. 2026;347(3):121548. doi:10.1016/j.engstruct.2025.121548.
26. Matanmi FO, Su Q, Gu M, Xu S, Liu F, Huang L, et al. Full-scale study on flexural behavior of high-strength steel–UHPC composite beam with modified clothoid-shaped dowels as shear connector. Eng Struct. 2026;348(6):121708. doi:10.1016/j.engstruct.2025.121708.
27. Wang Q, Guo S, Chen G, Lu C. Axial compressive behavior and stress-strain model of CFRP-UHPC composite-strengthened concrete columns. J Build Eng. 2026;120(12):115501. doi:10.1016/j.jobe.2026.115501.
28. Wang C, Yang J, Li G, Xie T, Deng K, Xu T. Experimental study and analysis of UHPC-RC composite multi-column frame piers. Structures. 2025;82(8):110479. doi:10.1016/j.istruc.2025.110479.
29. Satıoğlu AC, Bhardwaj SR. Numerical modelling of explosive spalling resistant ultra high performance concrete (UHPC) columns under fire loading. J Build Eng. 2026;117(5):114716. doi:10.1016/j.jobe.2025.114716.
30. Zeng X, Wang H, Han Z, Pan P, Deng K. Rehabilitation of damaged ECC-NC composite column using UHPC jacket. Eng Struct. 2026;351(9):122099. doi:10.1016/j.engstruct.2026.122099.
31. Jiang H, Li J, Gao Y, Zhang LF, Fang H, Chen Z, et al. Shear strengthening of reinforced concrete (RC) beams using ultra-high performance concrete (UHPC) jacketing: experimental analyses and calculation models. J Build Eng. 2026;118:114938. doi:10.1016/j.jobe.2025.114938.
32. Weng KF, Zhu JX, Huang BT, Dai JG, Chen JF. Shear strengthening of reinforced concrete beams using FRP-UHPC composite layer. Compos Struct. 2026;378(5861):119931. doi:10.1016/j.compstruct.2025.119931.
33. Hu X, Xue W, Xue W, Jiang J. Bond strength of sand-coated deformed GFRP bars in UHPC, HPC, and NC. Constr Build Mater. 2023;403(8):133175. doi:10.1016/j.conbuildmat.2023.133175.
34. Hu X, Xue W, Xue W. Bond properties of GFRP rebars in UHPC under different types of test. Eng Struct. 2024;314(9):118319. doi:10.1016/j.engstruct.2024.118319.
35. Wang R, Ma B, Chen X. Experimental study on bond performance between UHPC and steel bars. J Build Eng. 2023;79:107861. doi:10.1016/j.jobe.2023.107861.
36. Yoo DY, Shin HO. Bond performance of steel rebar embedded in 80–180? MPa ultra-high-strength concrete. Cem Concr Compos. 2018;93(6):206–17. doi:10.1016/j.cemconcomp.2018.07.017.
37. Hu X, Xue W, Lv Y. Bond properties between lapped steel rebars and UHPC under direct tension. Constr Build Mater. 2023;408(6):133761. doi:10.1016/j.conbuildmat.2023.133761.
38. GB/T 228.1-2010. Metallic materials—tensile testing part 1: method of test at room temperature. Beijing, China: Ministry of Housing and Urban-Rural Development of the People's Republic of China; 2010.
39. GB/T 50080-2016. Standard for test method of performance on ordinary fresh concrete. Beijing, China: Ministry of Housing and Urban-Rural Development of the People's Republic of China; 2016.
40. GB/T 50152-2012. Standard for test method of concrete structures. Beijing, China: Ministry of Housing and Urban-Rural Development of the People's Republic of China; 2012.
41. Wang L, Yi J, Zhang J, Jiang Y, Zhang X. Effect of corrosion-induced crack on the bond between strand and concrete. Constr Build Mater. 2017;153(3):598–606. doi:10.1016/j.conbuildmat.2017.07.113.
42. Wu Z, Deng M, Zhang Y, Chen H, Liu J, Tian T. Bond behavior of plain bar in highly ductile fiber-reinforced concrete (HDC) subjected to monotonic and repeated loading. J Build Eng. 2023;72(1):106593. doi:10.1016/j.jobe.2023.106593.
43. Liu H, Ma D, Wang Y, Guo Z, Jia M, Wu Z, et al. Experimental and analytical study of bond-slip behavior of ETS GFRP bar-to-concrete joints subjected to elevated temperatures. Eng Struct. 2025;343(3):121085. doi:10.1016/j.engstruct.2025.121085.

44. Liu Y, Zhang J, Zhao D, Tao X, Zhang M. Bond-slip response of ultrahigh-strength steel bars with spiral grooves embedded in reinforced concrete. Structures. 2024;70(7):107646. doi:10.1016/j.istruc.2024.107646.
45. Li H, Yang Y, Wang X, Tang H. Effects of the position and chloride-induced corrosion of strand on bonding behavior between the steel strand and concrete. Structures. 2023;58(3):105500. doi:10.1016/j.istruc.2023.105500.
46. Zhao J, Yin L, Li X, Yue X. Bond behavior of plain bars in concrete under reversed cyclic loading. Materials. 2023;16(13):4836. doi:10.3390/ma16134836.
47. Xiao F, Chen S, Wang J, Yang J, Yan D. Bond behavior of glass fiber–reinforced polymer bars with different surface geometries to seawater–sea sand concrete under FRP confinement. J Mater Civ Eng. 2025;37(8):04025232. doi:10.1061/jmcee7.mteng-19377.
48. Niyazuddin BU. Experimental investigation on bond behaviour of the GFRP bars with normal and high strength geopolymer concrete. Constr Build Mater. 2024;429:136395. doi:10.1016/j.conbuildmat.2024.136395.
49. Wang M, Wang Y, Chen G. Bond-slip law for the analysis of ribbed steel-FRP composite bars embedded into FRP-confined concrete. Eng Struct. 2025;339:120672. doi:10.1016/j.engstruct.2025.120672.
50. Lou GB, Hou J, Qi HH, Song ZH, Li GQ. Mechanical properties and bonding strength of twisted wire strands at elevated temperatures. J Constr Steel Res. 2024;213(2):108392. doi:10.1016/j.jcsr.2023.108392.
51. Xiong X, He L, Zhou Z, Xiao Q. The bond-slip constitutive model of retard-bonded prestressing steel strand. Constr Build Mater. 2023;365(4):129995. doi:10.1016/j.conbuildmat.2022.129995.